Influence of the Lattice Potential on the Electronic Structure of Metallic Interfaces: Dipole Effects

ALAN J. BENNETT AND C. B. DUKE*
General Electric Research and Development Center, Schenectady, New York 12301
(Received 26 June 1969)

We investigate the influence of the electronic energy-band structure on the self-consistent charge density and potential at solid-vacuum interfaces. A Kronig-Penny model in which the potential due to the positive ions is simulated by planar attractive δ-function potentials is used to describe the electron-ion interactions. The magnitude of the exchange-correlation potential is held fixed throughout the self-consistent calculation. Outside the surface, the charge density responsible for the Hartree potential is given by the actual electron density. Inside the surface it is given by the difference between the actual electron density and the electron density which would exist if no surface were present. In general, lattice-potential-induced alterations of the free-electron (i.e., uniform) bulk charge density may result in a substantial (e.g., 50%) decrease in the size of the surface dipole potential. This decrease is caused by the occurrence of smaller charge deviations at the surface. The magnitude of these deviations is influenced strongly by relatively small changes in the parameters of the model. One-dimensional models predict substantially larger charge deviations than those obtained using three-dimensional models.

I. INTRODUCTION

IT has been recognized for many years that the surface properties of a metal, as contrasted to its bulk (transport and equilibrium) properties, are dominated by the interactions of the conduction electrons with each other rather than with the lattice potential.[1–3] This recognition has motivated the (exclusive) use of jellium models to study the properties of metallic interfaces.[4–14] In this paper we examine a simplified Kronig-Penny description of the influence of the lattice potential on the charge density and electrostatic potential near a metal-vacuum interface. Although the effects of the electron-electron interactions predominate in the surface region, the results reported herein indicate that a periodic lattice potential can alter the surface dipole potential energy by as much as a factor of 2, relative to its value for a structureless, "jellium," model of the ion-core charge density.

Our model is motivated by noting, in analogy to models of low-energy electron diffraction[15–17] (LEED), that the lattice potential causes two geometrically distinct alterations of a jellium charge density. Consider the lattice to be described as a series of periodically repeating scattering planes parallel to the surface. Treating these planes as "structureless" leads to Darwin models of LEED intensity profiles which describe the primary Bragg peaks in these profiles.[16–20] This model is the one studied below. It provides an adequate description of periodic variations in the electronic charge density normal to the surface. The geometrical structure of the individual ion cores within each scattering plane leads to the spot pattern characteristic of LEED intensities[21] and to both multiple-scattering[17,22] and fractional-order[16,17,22] resonances in the intensity profiles associated with each spot. It also causes the charge density of the valence electrons to vary periodically within the surface plane, an effect which is neglected in this paper. The large kinetic energy associated with these charge-density oscillations is thought to cause them to be smoothed out in the surface layer of the metals.[3,5] However, their neglect constitutes a substantial deficiency in the model.

Our objective in this paper is an assessment of the order-of-magnitude effect on the surface charge density and work function caused by uniform planes of "ion-core" scattering charge. To achieve this objective, in Sec. II we reformulate the local-density approximation[3,10,11] to the self-consistent calculation of the surface charge density in order to incorporate the electron-lattice potential due to these scattering planes. In this section we also outline an approximate evaluation of the surface charge density using an analytically solvable one-electron model to define the basis states in the presence of an exchange-correlation potential alone.

* Permanent address: Dept. of Physics, University of Illinois, Urbana, Ill.
[1] E. Wigner and J. Bardeen, Phys. Rev. **48**, 84 (1935).
[2] J. Bardeen, Surface Sci. **2**, 381 (1964).
[3] C. B. Duke, J. Vac. Sci. Tech. **6**, 156 (1969).
[4] J. Bardeen, Phys. Rev. **49**, 653 (1936).
[5] R. Smoluchowksi, Phys. Rev. **60**, 661 (1941).
[6] H. Y. Fan, Phys. Rev. **61**, 365 (1942); **62**, 388 (1942).
[7] H. J. Juretschke, Phys. Rev. **92**, 1140 (1953).
[8] A. Sugiyama, J. Phys. Soc. Japan **15**, 965 (1960).
[9] T. L. Loucks and P. H. Cutler, J. Phys. Chem. Solids **25**, 105 (1964).
[10] A. J. Bennett and C. B. Duke, Phys. Rev. **160**, 541 (1967); **162**, 578 (1967).
[11] A. J. Bennett and C. B. Duke, in *The Structure and Chemistry of Solid Surfaces* (John Wiley & Sons, Inc., New York, 1969).
[12] R. W. Davies, Surface Sci. **11**, 419 (1968).
[13] J. W. Gadzuk, Surface Sci. **11**, 465 (1968).
[14] J. R. Smith, Phys. Rev. **181**, 522 (1969).
[15] J. L. Beeby, J. Phys. **C1**, 82 (1968).
[16] C. B. Duke and C. W. Tucker, Jr., Surface Sci. **15**, 231 (1969).
[17] C. B. Duke, J. R. Anderson, and C. W. Tucker, Jr., Surface Sci. (to be published).
[18] C. G. Darwin, Phil. Mag. **27**, 315 (1914).
[19] E. G. McRae, Surface Sci. **11**, 479 (1968); **11**, 472 (1968).
[20] R. O. Jones and J. A. Strozier, Jr., Phys. Rev. (to be published).
[21] C. Davisson and L. H. Germer, Phys. Rev. **30**, 705 (1927).
[22] E. G. McRae, J. Chem. Phys. **45**, 3258 (1966).

In Sec. III we present results for our model "metal" as well as for a one-dimensional model in which the distinction between a metal and an "insulator" can be made. We conclude in Sec. IV with a synopsis of our conclusions.

II. DEFINITION OF MODEL

A. Model Hamiltonian

The Hamiltonian describing the behavior of electrons in metals (at zero temperature) can be written schematically as

$$\mathcal{H}=\mathcal{H}_{ee}+V_{e\text{-ion}}, \tag{2.1a}$$

$$\mathcal{H}_{ee}=\sum_i\left(\frac{-\hbar^2\nabla^2}{2m}\right)+\tfrac{1}{2}\sum_{i\neq j}\frac{e^2}{|\mathbf{r}_i-\mathbf{r}_j|}, \tag{2.1b}$$

$$V_{e\text{-ion}}=\sum_{i,n}V(\mathbf{r}_i-\mathbf{R}_n), \tag{2.1c}$$

for electrons with position coordinates $\mathbf{r}_i$ moving in the electrostatic field of ion cores at the positions $\mathbf{R}_n$. Spin quantum numbers are suppressed throughout since we do not consider spin-dependent interactions. Techniques for reducing the solutions of Eqs. (2.1) to a tractable procedure have been reviewed both for the calculation of bulk band structures[23,24] and of surface properties.[2,3,25] For simplicity and clarity, we confine our attention to the treatment of $\mathcal{H}_{ee}$ in the (self-consistent) local-density approximation.[3,10,26] In this approximation, the influence of the electron-electron interactions on the motion of a given electron is described by a one-electron potential V_{ec}, which depends on the local electron density $n_e(\mathbf{r})$. The functional dependence of V_{ec} on n_e is specified by using various models for the correlation energy as described by Kohn and Sham[26] and by Bennett and Duke.[3,10] We consider the ion core centered about $\mathbf{R}_n$, to be described by a static charge distribution $n_i(\mathbf{r}-\mathbf{R}_n)$, and evaluate its influence on the electronic motion in the Hartree approximation.[24] Using these model simplifications, Eqs. (2.1) become the set of coupled one-electron equations

$$\{-\hbar^2\nabla^2/2m+V_{ec}[n_e(\mathbf{r})]+V_{ei}(\mathbf{r})-E\}\Psi_E(\mathbf{r})=0, \tag{2.2a}$$

$$n_e(\mathbf{r})=\sum_{E<E_F}|\Psi_E(\mathbf{r})|^2, \tag{2.2b}$$

$$\nabla^2V_{ei}(\mathbf{r})=4\pi e^2[\sum_i n_i(\mathbf{r}-\mathbf{R}_i)-n_e(\mathbf{r})], \tag{2.2c}$$

$$\int d^3r[n_e(\mathbf{r})-\sum_i n_i(\mathbf{r}-\mathbf{R}_i)]=0, \tag{2.2d}$$

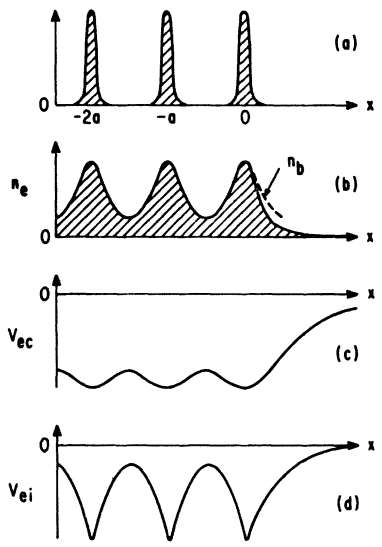

FIG. 1. Schematic diagram of the positive charge density (a), electron charge density (b), exchange-correlation potential (c), and electron-ion potential (d) near a metal-vacuum interface. The dashed line in (b) indicates the periodic component of the electron density in the exterior cell. The positive charge background is assumed to be uniform sheets at $x_n=-na$, $n\geq 0$. The geometrical "surface" of the solid is at $x=\frac{1}{2}a$. The V_{ec} curves are sketched for the case that the maximum value of n_e is less than or equal to 10^{22} cm^{-3} (see Fig. 4 of Ref. 3).

which are to be solved self-consistently. The bulk Fermi energy is denoted by E_F.

The solution of Eqs. (2.2) for a given ion-core charge density n_i, and lattice geometry $\{R_i\}$, provides both an energy-band structure of the "bulk" and a description of its surface properties. We wish to achieve only the more modest goal of estimating the influence on the surface properties of various (prescribed) electron-lattice interactions. In order to visualize the ingredients of an appropriate model description, we show in Fig. 1 a schematic diagram of both V_{ec} and V_{ei} for the $n_i(\mathbf{r})$ associated with uniform sheets of charge parallel to the surface. The major deviations of the charge density from the bulk (i.e., periodic) values occur in the exterior cell ($-\frac{1}{2}a\leq x\leq\frac{1}{2}a$). Let us decompose both V_{ei} and V_{ec} into bulk and surface parts:

$$V_{ei}=V_b+V_d, \tag{2.3a}$$

$$V_{ec}=V_{ec,b}+V_{ec,s}. \tag{2.3b}$$

The bulk potentials V_b and $V_{ec,b}$ together with the band structure of the material are obtained from the solutions to Eqs. (2.2) using periodic boundary conditions. In this limit, Eqs. (2.2) exhibit Bloch-function solutions $\Psi_{n\mathbf{k}}(\mathbf{r})$ defined by

$$\{-\hbar^2\nabla^2/2m+V_{ec,b}[n_b(\mathbf{r})]+V_b(\mathbf{r})-\epsilon_n(\mathbf{k})\}\times\Psi_{n\mathbf{k}}(\mathbf{r})=0, \tag{2.4a}$$

[23] F. Herman, Rev. Mod. Phys. **30**, 102 (1958).
[24] W. A. Harrison, *Pseudopotentials in the Theory of Metals*, (W. A. Benjamin, Inc., New York, 1966).
[25] C. B. Duke, *Tunneling in Solids* (Academic Press Inc., New York, 1969), Chap. 3.
[26] W. Kohn and L. J. Sham, Phys. Rev. **140**, A1133 (1965); **145**, 561 (1966).

$$\nabla^2 V_b = 4\pi e^2\{\sum_i n_i(\mathbf{r}-\mathbf{R}_i) - n_b(\mathbf{r})\}, \quad (2.4b)$$

$$n_b(\mathbf{r}) = \sum_{\epsilon(\mathbf{k})\leq E_F} |\Psi_{n\mathbf{k}}(\mathbf{r})|^2. \quad (2.4c)$$

We perform our estimate of the influence of the lattice potential on the electronic structure of the surface by using the dipole approximation.[4,10] Using Eqs. (2.3) we *define*

$$V_{ec}[n_e(\mathbf{r})] \equiv V_{ec,b}[n_b(\mathbf{r})]\theta(\tfrac{1}{2}a-x) + V_{ec,s}(\mathbf{r}), \quad (2.5a)$$

$$V_{ei}(\mathbf{r}) = V_b(\mathbf{r})\theta(\tfrac{1}{2}a-x) + V_d(\mathbf{r}). \quad (2.5b)$$

The surface "dipole" potential is given by

$$\nabla^2 V_d(\mathbf{r}) = 4\pi e^2[n_b(\mathbf{r}) - n_e(\mathbf{r})], \quad (2.5c)$$

and $V_{ec,s}(\mathbf{r})$ will be specified below. The important feature of this approximation is that the sole entrance of the bulk band structure into the determination of the surface potential is via the occurrence of $n_b(\mathbf{r})$ in Eq. (2.5c). Therefore, once Eqs. (2.4) have been solved self-consistently, their only role in determining the dipole potential V_d occurs via their specification of the "effective" positive background charge $n_b(\mathbf{r})$ in the absence of a surface. This result motivates the construction of our model problem in which the bulk potential is prescribed *a priori* by a Kronig-Penny model,

$$V_{ec,b}[n_b(\mathbf{r})] + V_b(\mathbf{r}) \equiv V(x) = -U_0 + \left(\frac{\hbar^2\gamma^2\alpha}{m}\right)\sum_{n=0}^{\infty}\delta(x+na), \quad (2.6)$$

in which $(U_0+\hbar^2\gamma^2/m)$ is the average value of the potential[10] of the bulk material. Using this model, Eqs. (2.2) become those which we shall solve numerically:

$$\Psi_E(\mathbf{r}) = (e^{i\mathbf{k}_{||}\cdot\rho}/\sqrt{A})\chi_{E_x}(x), \quad (2.7a)$$

$$E = E_x + \hbar^2 k_{||}^2/2m, \quad (2.7b)$$

$$\left[\frac{-\hbar^2}{2m}\frac{d^2}{dx^2} + V(x) + V_d(x) + V_{ec,s}(x) - E_x\right]\times\chi_{E_x}(x) = 0, \quad (2.7c)$$

$$d^2V_d/dx^2 = 4\pi e^2[n_b(x) - n_e(x)], \quad (2.8a)$$

$$n_e(x) = \frac{m}{2\pi^2\hbar^2}\int_0^{E_F} dE_x(E_F-E_x)\times\left(\frac{\partial k}{\partial\epsilon}\right)|\chi_{E_x}(x)|^2, \quad (2.8b)$$

$$\left[\frac{-\hbar^2}{2m}\frac{d^2}{dx^2} + V(x) - \epsilon_n(k)\right]\chi_{nk}(x) = 0, \quad (2.9a)$$

$$n_b(x) = \frac{m}{\pi^2\hbar^2}\int_0^{E_F} d\epsilon(E_F-\epsilon)\frac{\partial k}{\partial\epsilon}|\chi_{nk}(x)|^2. \quad (2.9b)$$

Equations (2.6)–(2.9) define the calculation of the surface potential V_d and electronic charge density n_e in the presence of a surface at $x=\frac{1}{2}a$ for a specified bulk periodic potential given by Eq. (2.6), with solutions specified by Eqs. (2.9) plus periodic boundary conditions. The requirement that no dipole moment exists across the bulk solid uniquely determines the truncation of $n_b(x)$ at $x=\frac{1}{2}a$.

We use the limit of a semi-infinite continuum so that, for a free-electron material, we have

$$E_F = \hbar^2(3\pi^2\bar{n})^{2/3}/2m, \quad (2.10)$$

in which $\bar{n}$ is the average electron density per unit volume.[3,10] The wave functions are normalized by requiring that in the limit of a uniform, infinite lattice, we have

$$\chi_{nk}(x) = e^{ikx}u_{nk}(x), \quad (2.11a)$$

$$u_{nk}(x+a) = u_{nk}(x), \quad (2.11b)$$

$$\int_{\text{cell}} |u_{nk}(x)|^2 dx = 1. \quad (2.11c)$$

The solution of Eq. (2.7c) in the presence of a surface at $x=\frac{1}{2}a$ is described in Secs. II B and II C. Here, we only need to observe that Eqs. (2.11) suffice to specify the normalization in this more general case also.

B. Basis States in the Absence of a Periodic Potential

We already have noted that in carrying out self-consistent-field calculations in the absence of the lattice potential, it is convenient to use a model one-electron potential for which the Schrödinger equation can be solved analytically. This procedure permits the calculation of charge densities by simple quadrature, and the use of the parameters of the potential as variational parameters in the iteration process.[10,11] We also impose the requirement that the potential be an analytic function of position in order to eliminate the possibility of spurious oscillations in the charge density associated with joining conditions on the wave function.[27]

A suitable potential proposed by Eckart[28] is given by

$$V_0(x) = -A\xi(1-\xi)^{-1}, \quad (2.12a)$$

$$\xi = -e^{(x-x_0)/s}. \quad (2.12b)$$

We are interested in the nondegenerate continuum of solutions to Eq. (2.7c) in the absence of a lattice potential:

$$\left(\frac{-\hbar^2}{2m}\frac{d^2}{dx^2} + V_0(x) - \frac{\hbar^2k^2}{2m}\right)\chi_k^{(0)}(x) = 0. \quad (2.13)$$

[27] M. E. Alferieff and C. B. Duke, J. Chem. Phys. 46, 938 (1967).
[28] C. Eckart, Phys. Rev. 35, 1303 (1930).

The bounded eigenfunctions of this equation, $E<A$, which decay exponentially for $x \gg x_0$, are given by[29,30]

$$\chi_k^{(0)}(x) = (-\xi)^{iks}(1-\xi)^{-iks-\eta} \times F[iks+\eta,\ 1+iks+\eta,\ 1+2\eta,\ (1-\xi)^{-1}], \quad (2.14a)$$

$$k^2 = 2mE_x/\hbar^2, \quad (2.14b)$$

$$\eta^2 = 2ms^2(A-E_x)/\hbar^2, \quad (2.14c)$$

in which $F(a,b;c,z)$ denotes the Gauss hypergeometric function.[29] The Jost-function solutions which become plane waves as $x \longrightarrow -\infty$ are given by

$$\phi_k^{(\pm)}(x) = (-\xi)^{\pm iks} F(\pm iks-\eta,\ \pm iks+\eta,\ 1\pm 2iks,\ \xi) \longrightarrow e^{\pm ikx} \quad \text{as} \quad x \longrightarrow -\infty. \quad (2.15)$$

The bounded eigenfunction, (2.14a), is a linear combination of the Jost functions described by Bennett and Duke.[10] The Jost functions are utilized in Sec. II C as the appropriate one-electron basis states in terms of which the wave function in the regions between the δ functions in a Kronig-Penny model can be expressed.

C. Envelope-Function Approximation

Our model iterative solution to Eqs. (2.7) is based on taking

$$V(x)+V_d(x)+V_{ec,s} \equiv V_0(x)+\left(\frac{\hbar^2\gamma^2 a}{m}\right)\sum_{n=0}^{\infty}\delta(x+na) \quad (2.16)$$

in Eq. (2.7c). The "inner-potential" $V_0(x)$ is defined by Eqs. (2.12). The dipole contributions to the surface potential are obtained by determining $V_d(x)$ from Eqs. (2.8) via an iterative procedure.

Our immediate task in this subsection is the solution of Eq. (2.7c) using Eqs. (2.12) and (2.16) to specify the potential as a function of the four parameters A, s, x_0, and γ. Unfortunately, we have not succeeded in obtaining an exact solution for the wave functions. The wave function is written as

$$\chi_{E_x}(x) = \phi_k^{(+)}(x)u_k(x)+e^{ib}\phi_k^{(-)}(x)u_{-k}(x), \quad x<a/2; \qquad = R\chi_k^{(0)}(x), \quad x>\tfrac{1}{2}a. \quad (2.17)$$

The Jost functions $\phi_k^{(\pm)}$ are defined to be the solutions to Eq. (2.13), in which k is an *undetermined parameter* to be chosen conveniently at a subsequent stage of the analysis. Insertion of Eqs. (2.17) into Eq. (2.7c) gives the equation satisfied by the functions $u_k(x)$:

$$\left[\frac{d^2}{dx^2}+2\left(\frac{d}{dx}\ln\phi_k^{(\pm)}\right)\frac{d}{dx}+(\alpha^2-k^2) -2\gamma^2 a\sum_{n=0}^{\infty}\delta(x+na)\right]u_{\pm k}(x)=0, \quad (2.18)$$

$$\alpha^2 = 2mE_x/\hbar^2. \quad (2.19)$$

In general, $\ln\phi_k^{(\pm)}$ is a nonlinear function of x, so that Eq. (2.18) assumes a complex form. However, the coefficient of the du/dx term in Eq. (2.18) may be expanded according to

$$\ln\phi_k^{\pm} = ikx+O(x^2), \quad (2.20)$$

in which the terms $O(x^2)$ are nonzero only near $x \cong \frac{1}{2}a$. The envelope-function approximation is defined by neglecting the terms $O(x^2)$ in (2.20). Evidently these terms may be taken into account using perturbation theory by treating

$$2\left(\frac{d\ln\phi_k^{\pm}}{dx}\mp ik\right)\frac{du_{\pm k}^{(0)}}{dx}$$

as the source term for an inhomogeneous equation for a correction term $u_{\pm k}^{(1)}$. This zeroth-order term $u_{\pm k}^{(0)}$ is obtained by use of the envelope-function approximation. As we shall use $s \sim x_0 \sim a$ in Eq. (2.12b), we expect $u^{(1)}$ to be small except possibly in the cell at the interface.

By use of the envelope-function approximation, we have reduced Eq. (2.18) to that for the cell-periodic part of the Bloch functions in a Kronig-Penny model. Thus the envelope-function approximation defines a sort of generalized effective-mass approximation,[31] in which the wave-vector dependence of the cell-periodic functions is not neglected. This generalization is crucial in our problem because the charge density is comprised of a superposition of the moduli of wave functions associated with **k** vectors from large regions of the Brillouin zone. In addition, the solutions to the one-dimensional Kronig-Penny model with δ potentials have been studied extensively.[32–34] Therefore, the results for the $u_k^{(0)}(x)$ are readily available and are

[29] F. Oberhettinger, in *Handbook of Mathematical Functions*, edited by M. Abramowitz and I. A. Stegun (U. S. Dept. of Commerce, National Bureau of Standards, Washington, D. C., 1964), Appl. Math. Ser. 55, p. 555.

[30] The result (2.14) is obtained by introducing the variable substitution (2.12b) into Eq. (2.13) and writing

$$\chi = \exp[iks\ln(\xi)]F(\xi).$$

One finds immediately that $F(\xi)$ satisfies the hypergeometric equation. The solution (2.14a) in the text is the exponentially decaying series expansion about the singular point $\xi=\infty$. It is given by Eq. (15.5.8) in Ref. 29, from which Eq. (2.14) is obtained by use of Eq. (15.3.4) in Ref. 29. Equation (15.5.13) contained in Ref. 29, which purports to give (2.14) directly, is in error.

[31] W. Kohn, Solid State Phys. **5**, 238 (1957).

[32] D. S. Saxon and R. A. Hunter, Phillips Res. Rept. **4**, 82 (1949).

[33] E. Aerts, Physica **26**, 1047 (1960); **26**, 1063 (1960).

[34] P. Schnupp, Solid State Electron. **10**, 785 (1967); Phys. Status Solidi **21**, 567 (1967).

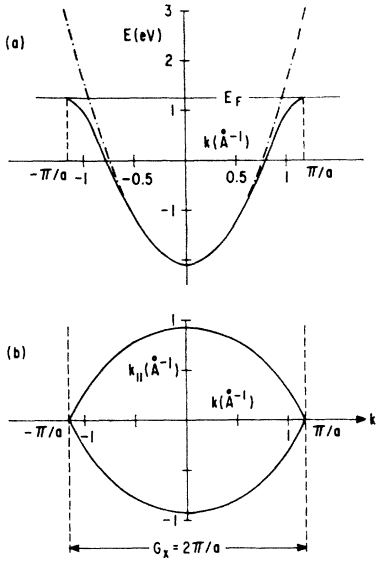

FIG. 2. (a) Solid line shows the electron energy versus momentum perpendicular to the junction for the Kronig-Penny model used to represent a hypothetical metal. The dashed curve shows free-electron behavior. The latter curve has been shifted to remove the effects of the averaged δ-function potentials. (b) Fermi surface of the model metal.

given by

$$u_k^{(0)}(x)=N_k e^{-ik(x+na)}[\sin\alpha(x+na) - e^{-ika}\sin\alpha(x+na-a)], \quad -na-\tfrac{1}{2}a\leq x\leq -na+\tfrac{1}{2}a; \quad (2.21a)$$

$$N_k=-\left[1-\frac{\sin 2\alpha a}{2\alpha a} -\cos ka\left(\cos\alpha a-\frac{\sin\alpha a}{\alpha a}\right)\right]^{1/2}, \quad (2.21b)$$

for the normalization specified by (2.11c). Equations (2.17) and (2.21) specify a solution to Eq. (2.18) if and only if k is related to the energy E_x [i.e., the parameter α defined by (2.19)] via[32]

$$\cos ka=\cos\alpha a+(\gamma^2 a/\alpha)\sin\alpha a. \quad (2.22)$$

In the case of bulk band-structure calculations, the parameter k is determined from periodic boundary conditions so that Eq. (2.22) determines[32] the $E_x(k)$ $\equiv\epsilon_n(k)$ dispersion relation to be used in Eqs. (2.9). In our case, k is treated as a continuous index whose integration range is specified by the restriction

$$E_F\geq\epsilon_n(k) \quad (2.23)$$

in Eqs. (2.8b) and (2.9b) for the density.

D. Wave Functions and Electron Densities

The electron density defined by Eq. (2.8b) is obtained using wave functions of the form given in Eq. (2.17), in which R and δ are determined by continuity of χ and $d\chi/dx$ at $x=\frac{1}{2}a$. The $\chi_k^{(0)}$, $\phi_k^{(\pm)}$, and $u_k^{(0)}$ are specified by Eqs. (2.14), (2.15), and (2.21), respectively. If we define

$$\chi_k^{(\pm)}\equiv\phi_k^{(\pm)}(x)u_{\pm k}^{(0)}(x), \quad (2.24)$$

we obtain the formulas used in our numerical calculations:

$$e^{i\delta}=[W(\chi^{(0)},\chi^{(+)})/W(\chi^{(-)},\chi^{(0)})]_{x=a/2}, \quad (2.25a)$$

$$R=[W(\chi^{(-)},\chi^{(+)})/W(\chi^{(-)},\chi^{(0)})]_{x=a/2}, \quad (2.25b)$$

$$W(\chi_1,\chi_2)=\chi_1\frac{d\chi_2}{dx}-\chi_2\frac{d\chi_1}{dx}. \quad (2.25c)$$

The hypergeometric functions used in $\chi_k^{(0)}$ and $\phi_k^{(\pm)}$ are evaluated directly from the Gauss hypergeometric series.[29] If the argument of one of these functions becomes greater than unity, then one of the variable substitutions given by Eqs. (15.3.4) or (15.3.5) in Ref. 29 is used to reduce the argument to a value inside the circle of convergence for the Gauss series. The $u_k^{(0)}(x)$ are evaluated directly from Eqs. (2.21). The densities $n_e(x)$ and $n_b(x)$ are evaluated by numerical performance of the integrals in Eqs. (2.8b) and (2.9b).

III. NUMERICAL RESULTS AND CONCLUSIONS

A. General Results

Before presenting detailed computations, let us first survey the basic results obtained. At both jellium and metal surfaces a dipole potential, due to the "spreading" of electronic charge into the vacuum, occurs. It raises the work function of the material. However, any real metal surface is microscopically rough because of its characteristic protrusion of atoms into the vacuum. Therefore, a reverse dipole is formed by the smoothing of the electronic charge density.[3,5] When the microscopic roughness of the surface is ignored, as in our model, there are two principal effects which distinguish between the results obtained for the metal-vacuum interface and those for the jellium-vacuum interface.

First, as may be seen from Eq. (2.5c), the size of the dipole potential roughly scales with the size of the difference between the actual electron charge density calculated for the finite sample and the electron density which would exist in the sample if no surface were present. The charge deviation is confined to a region close to the surface, and the surface is at the point $\frac{1}{2}a$ (a is the lattice constant), where the undisturbed charge density has a minimum. Thus, for attractive lattice potentials [$\gamma^2<0$ in Eq. (2.16)] the effective background charge density $n_b(x)$ near the surface is less than the constant charge density in a comparable jellium sample. This result tends to reduce the size of dipole at the metal-vacuum interface relative to that at the jellium-vacuum interface.

The second effect is due to the importance of the cosinelike wave functions associated with k vectors near the Brillouin-zone boundary which account for the pileup of electron density near the atoms (or sheets of positive charge in our model). Relative to lower-energy electrons, the large-k vector electrons are influenced by a small exchange-correlation potential. Therefore, these (high-energy) electrons preferentially spread into the vacuum. This result can cause changes in the charge density near the metal surface which are not present at the comparable jellium surface. In particular, the charge density at the site of the atom closest to the surface may be substantially reduced. This reduction tends via Eq. (2.5c) to increase the dipole layer over that at a jellium-vacuum surface. In three-dimensional models[3,10,11] a phase-space factor (E_F-E_x), associated with electrons moving parallel to the surface, appears in Eqs. (2.8b) and (2.9b) for the density. As emphasized by Bennett and Duke,[3,10] this phase-space weighting reduces the contribution of the high-energy electrons to the dipole potential. A more realistic model of the band structure might diminish the importance of the (E_F-E_x) factor. Therefore, we utilize a one-dimensional calculation in which (E_F-E_x) does not appear in the expressions for the density to illustrate the potential importance of this latter effect opposing the first one.

Sections III B and III C consist of a comparison of the jellium (free-electron)–vacuum junction results and the metal (non-free-electron material)–vacuum results for three-dimensional and one-dimensional models, respectively. The separation energy S_n, i.e., the amount of energy required to remove an electron from the system in the absence of the dipole potential, is chosen to be a function only of the average density and hence is not affected by the lattice potential. In particular, the lowering[3] of the electron-dispersion curves due to the averaged δ-function potentials is ignored.

B. Three-Dimensional Model

In order to estimate the difference between the dipole potentials and charge densities at a metal-vacuum interface and those at a jellium-vacuum interface, we first consider a metal with lattice constant $a=2.75$ Å, in which the Fermi energy E_F is chosen equal to $\alpha(k_{\max}=\pi/a)$ as shown in Fig. 2. The strength of the attractive δ-function potentials of the Kronig-Penny model, γ^2, is chosen equal to -2.07×10^{16} in order to ensure a reasonable amount of deviation from free-electron behavior. Similar calculations are then performed with $\gamma=0$ and $\bar{n}=3.0$, i.e., for a comparable jellium-vacuum situation.

A self-consistent iteration scheme similar to that used in our previous work[3,10,11] is utilized. $V_0(x)$ [Eq. (2.16)] is represented by the Eckart potential [Eq. (2.12)] with the parameters A and x_0 chosen to represent the calculated potential at various stages of the iteration procedure. The width of the potential, s, is held fixed and equal to the "reasonable" value of 3 Å; A is chosen equal to the sum of S_n (the fixed separation energy) E_F and V_d (the over-all change in dipole potential across the surface); and x_0, as explained below, is adjusted to ensure charge neutrality. The iteration procedure consists of the following steps:

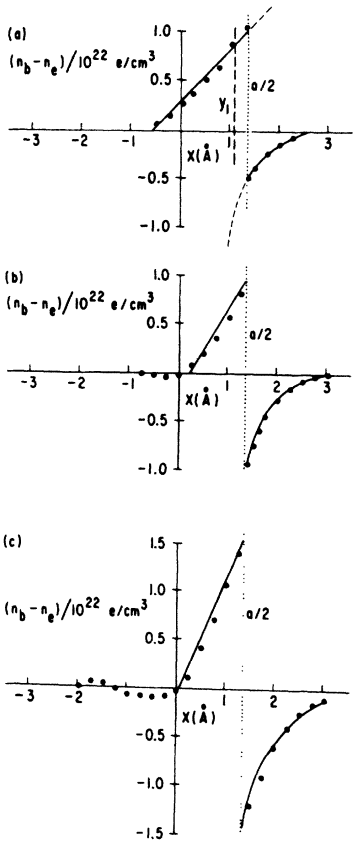

FIG. 3. (a) Example of the electron-density deviations obtained at an intermediate stage of the iteration procedure for a three-dimensional model of a metal-vacuum interface. The points are the calculated density deviations. The solid lines represent the linear model of the positive deviations and the exponential model of the negative deviations. The surface is originally taken to be at $x=\frac{1}{2}a$, but with the use of an analytic continuation (dashed lines) of the model deviations, its position is shifted to $x=y_1$ to assure change neutrality. The points shown in (b) denote the converged calculated density deviations at the $\bar{n}=3.0\times10^{22}$ e/cm^3 three-dimensional model of a metal-vacuum interface. The points in (c) denote the converged calculated density deviations at the $\bar{n}=3.0\times10^{22}$ e/cm^3 three-dimensional model of the jellium-vacuum interface. The solid curves in (b) and (c) represent the linear fit to the positive density deviations and the exponential fit to the negative density deviations.

(i) A starting potential is defined by

$$A=S_n(\bar{n})+E_F;\quad x_0=0,$$

where $\bar{n}$ is the average density deep inside the material and our previous jellium-model dependence[10] of S_n on $\bar{n}$ is used to obtain a value for the separation energy.

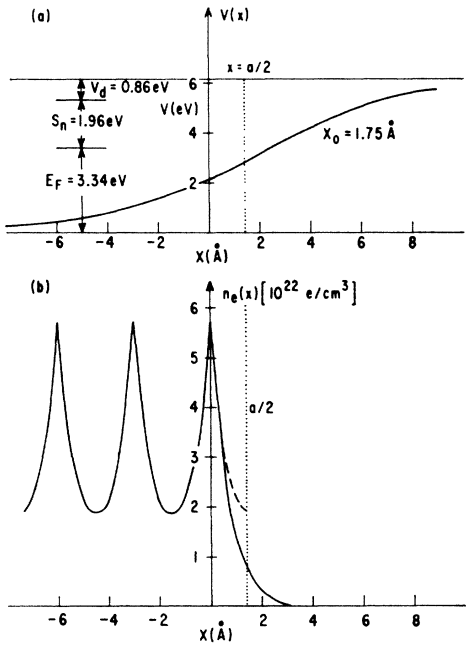

FIG. 4. (a) Converged model potential at the three-dimensional metal-vacuum interface with $\bar{n}=3.0\times10^{22}\ e/\text{cm}^3$. (b) The dashed line represents the charge density n_b in the material with no surface effects present. The solid line represents the converged calculated electron density n_e.

(ii) The electron densities $n_e(x)$ and $n_b(x)$ are calculated from Eqs. (2.8b) and (2.9b), respectively. The difference $[n_b(x)-n_e(x)]$ is plotted as shown in Fig. 3(a). The regions of positive and negative net effective charge are represented by "fitted" linear and exponential curves, respectively, as shown in Fig. 3(a). Each curve is extended across the boundary beyond its proper domain of definition and the actual position of the surfaces, y_1, is chosen to guarantee the integrated neutrality of the "effective" charge n_b-n_e.

(iii) The total change in potential across the junction, V_d, is calculated with the use of Eq. (2.5c) and the model charge deviations.

(iv) The potential to be used in the next iteration is defined by setting

$$A=S_n(\bar{n})+V_d+E_F$$

and

$$x_0=x_0-(y_1-\tfrac{1}{2}a).$$

Steps (ii)-(iv) are repeated until convergence is obtained. This occurs, in general, after approximately four iterations.

As noted elsewhere[10,11] the use of the model charge deviation is required to ensure proper convergence of the iterations. The particular model used here is chosen for convenience in treating the metal-vacuum interface. Although difference from that used previously[11] to treat the jellium-vacuum interface, it yields results similar to those obtained in that analysis.[11]

The converged calculated charge deviations and model deviations for the metal-vacuum interface are shown in Fig. 3(b). The model charge deviations provide a good representation of the calculated charge deviations. The converged model potential and electron density are shown in Figs. 4(a) and 4(b), respectively. The total change in the dipole potential across the surface is 0.86 eV.

The converged density deviations and model deviations for the jellium-vacuum interface are shown in Fig. 3(c). The converged model potential and electron density for this interface are shown in Figs. 5(a) and 5(b), respectively. The total change in dipole potential across the surface, 2.25 eV, is more than twice that present in the metal-vacuum case. This is largely due, as may be seen from Figs. 3(b) and 3(c), to the first effect of Sec. III A, i.e., the larger maximum charge deviation at the jellium surface.

The occurrence of Friedel oscillations in the charge density is evident in Fig. 5(b). They are larger in this case than in our previous analyses.[3,11] One reason for this result is the use in step (iii) of our present iteration procedure of a model potential, $V_d(x)$, which does not exhibit oscillations in the potential associated with oscillations in the charge density.

C. One-Dimensional Calculations

Calculations similar to those described in Sec. III B were performed for a one-dimensional jellium model

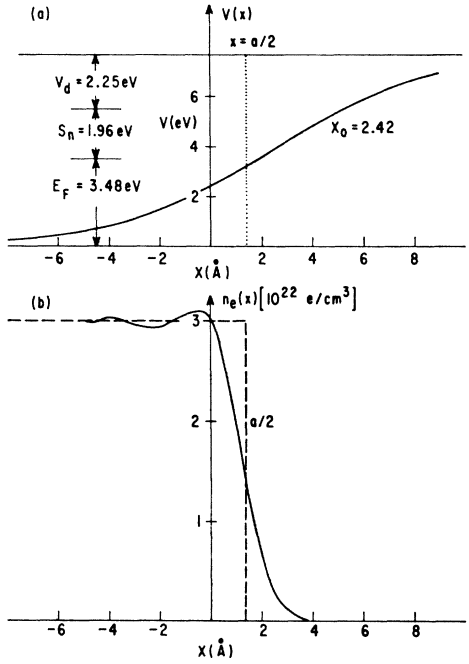

FIG. 5. (a) Converged model potential at the three-dimensional $\bar{n}=3.0\times10^{22}\ e/\text{cm}^3$ jellium-vacuum interface. (b) Dashed line represents the density in the material, n_b, with no surface effects present. The solid line represents the converged calculated electron density n_e.

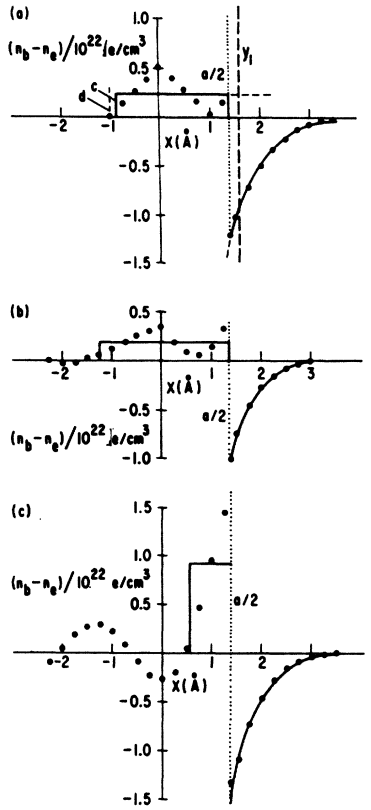

FIG. 6. (a) Example of the density deviation obtained at an intermediate stage of the iteration procedure for a one-dimensional interface. The points are the calculated density deviations. The solid lines represent the constant model of the positive deviations and the exponential model of the negative deviations. The surface is originally taken to be at $x=\frac{1}{2}a$. With the use of a continuation (dashed lines) of the model deviations, its position is shifted to $x=y_1$ to assure charge neutrality. The points in (b) are the converged calculated density deviations at the $\bar{n}=3.0\times10^{22}$ e/cm^3 one-dimensional model of a metal-vacuum interface. The points in (c) are the converged calculated density deviations at $\bar{n}=3.0\times10^{22}$ e/cm^3 one-dimensional jellium-vacuum interface. The solid lines in (b) and (c) represent the constant fit to the positive density deviations and the exponential fit to the negative density deviations.

in order to investigate the importance of the second effect of Sec. III A, i.e., the importance of the preferential spreading of zone-boundary wave functions into the vacuum. The iteration procedure used was similar to that described in Sec. III B. There were, however, two differences. The three-dimensional expressions for the densities, Eqs. (2.8b) and (2.9b), were replaced by

$$n_e(x)=\frac{C}{2\pi}\int_0^{E_F} dE_x\left(\frac{dk}{d\epsilon}\right)|\chi_{E_x}(x)|^2 \qquad (3.1)$$

and

$$n_b(x)=\frac{2C}{\pi}\int_0^{E_F}\frac{dk}{\delta\epsilon}dE_x|\chi_{nk}(x)|^2. \qquad (3.2)$$

The constant C was chosen such that the average density $\bar{n}$ calculated for the full band, i.e., $E_F=\alpha(k_{\max}=\pi/a)$ with $\gamma^2=-2.07\times10^{16}$, was equal to the density obtained in the full three-dimensional calculation [3.0×10^{22} cm^{-3}]. This makes possible a self-consistent calculation for the one-dimensional case which can be compared with that performed for the three-dimensional case.

A typical charge deviation found in step (ii) of the iteration procedure is shown in Fig. 6(a). The model charge deviation used to represent the numerical one also is shown in the figure. The model consists of a region of constant charge deviation and one of exponentially varying charge deviation. The constant value of the density deviation inside the material, ρ_1, is adjusted so that

$$\rho_1 x(\tfrac{1}{2}a-c)=\int_d^{a/2}[n_b(x)-n_e(x)]dx, \qquad (3.3)$$

where c, d, and the parameters of the exponential curves are fitted to the calculated points. As in the three-dimensional calculation, the model curves are extended across the boundary beyond their actual domain of definition, and a new position of the surface, y_1, is chosen to guarantee charge neutrality in the model system.

The converged density deviations, model potential, and electron density for the one-dimensional metal-vacuum interface are shown in Figs. 6(b), 7(a), and 7(b), respectively. The total change in dipole potential across the junction is 1.54 eV. The analogous quantities

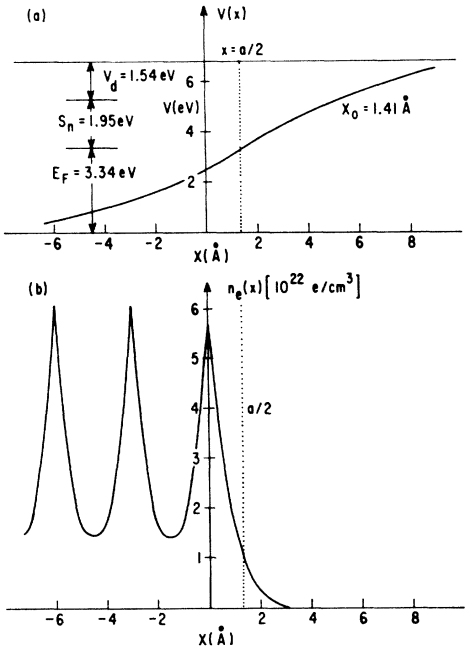

FIG. 7. (a) Converged model potential at the one-dimensional metal-vacuum interface with $\bar{n}=3.0\times10^{22}$ e/cm.^{3} (b) Converged calculated electron density at the interface [see Fig. 6(b) to obtain the periodic component of the density].

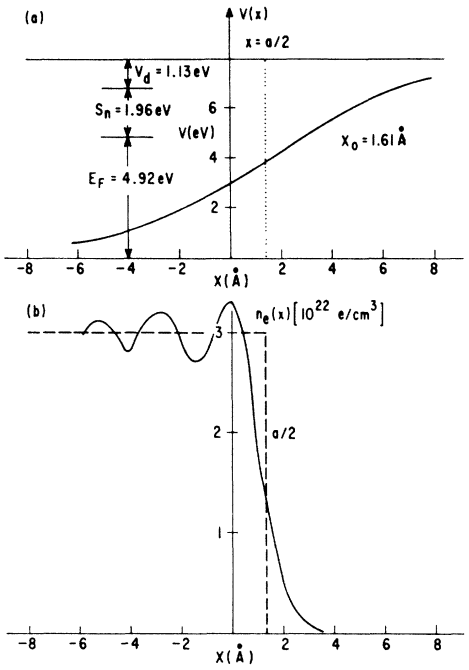

FIG. 8. (a) Converged model potential at the one-dimensional jellium-vacuum interface with $\bar{n}=3.0\times10^{22}\ e/\text{cm}^3$. (b) Dashed line represents the charge density n_b in the material with no surface effects present. The solid line represents the converged calculated electron density n_e.

at a one-dimensional jellium-vacuum interface are shown in Figs. 6(c), 8(a), and 8(b). The size of the dipole potential is within the accuracy of the calculation approximately the same as that found for the one-dimensional metal-vacuum surface.

A comparison of Figs. 6(b) and 6(c) shows that the maximum charge deviation is greater for the case of the jellium surface than for the model metal surface just as was true in the three-dimensional calculations of Sec. III B. Now, however, the zone-boundary electrons which preferentially spread into the vacuum contribute significantly to the charge density at the first plane of atoms (i.e., $x=0$). This causes a net positive charge deviation $[n_b(r)-n_e(r)]$ at the "center" of the first plane of atoms, thereby extending the charge density farther into the material than in the three-dimensional junctions, and simultaneously causing it to be an oscillating function of the penetration depth from the surface. These effects render the value of $n_e(\frac{1}{2}a)$ much less important in determining the value of the dipole potential then in the case of a small monotonically decreasing density deviation such as that shown in Fig. 3(a). Consequently, the local minimum in $n_b(x)$ at $x=\frac{1}{2}a$ is no longer effective in reducing the dipole potential from its value in a jellium model. This is a significant result because it shows how sensitive the charge density [and hence $V_d(x)$] is to the phase-space weighting factor $[E_F-E_x]$ in the three-dimensional model. It is precisely this sensitivity which led us to emphasize in previous analyses[3,10] the possibility of large charge-density redistributions at metal-semiconductor interfaces, in analogy to their occurrence at bimetallic interfaces. Comparison of Figs. 3 and 6 leads to the general conclusion that for one-dimensional models [within the framework of which Figs. 6(a), 6(b), and 7 represent results for a genuine "semiconductor"] the absence of phase-space restrictions on the high-energy eigenstates, $E_x\sim E_F$, leads to much larger charge deviations than occur in three-dimensional models. This pathological feature of one-dimensional models suggests that they are not suitable for studies of the electronic structure of solid interfaces.

IV. SUMMARY

The influence of band structure on the self-consistent charge density and dipole potential at solid-vacuum interfaces has been examined. Ignoring atomic structure parallel to the plane of the junction, we have used a simple planar Kronig-Penny model to represent the ion potentials. The exchange and correlation potentials are held fixed through the calculation. Only the charge deviations closest to the surface are considered, and those are represented by analytic forms at intermediate stages of the iteration procedure. This accounts for errors of perhaps 20% in our results, but enables us to identify and estimate two effects which differentiate the jellium-vacuum and metal-vacuum interfaces. The first effect, the smaller magnitude of the charge deviation at the metal surface, reduces the size of the dipole potential relative to that at the jellium surface. This result is clearly demonstrated in the three-dimensional model of Sec. III B. A second effect, the greater penetration into the material of the density deviation in the case of the metal, raises its dipole potential with respect to that at jellium surface. In the model used in Sec. III B, a phase-space factor largely eliminates this effect. However, the results of Sec. III C, where a one-dimensional model is used, show that for particular band structures, the second effect predominates. The dipole at a single-crystal surface of a metal is thus shown to depend on particular features of the metallic band structure, and on the details of the model used to describe this band structure.